ACS APPLIED MATERIALS & INTERFACES

Letter

www.acsami.org

Templated 3D Ultrathin CVD Graphite Networks with Controllable Geometry: Synthesis and Application As Supercapacitor Electrodes

Ben Hsia,[†] Mun Sek Kim,[†] Lunet E. Luna,[†] Nisha R. Mair, Yongkwan Kim, Carlo Carraro, and Roya Maboudian*

Department of Chemical and Biomolecular Engineering, University of California, Berkeley, California 94720, United States

Supporting Information

ABSTRACT: Three-dimensional ultrathin graphitic foams are grown via chemical vapor deposition on templated Ni scaffolds, which are electrodeposited on a close-packed array of polystyrene microspheres. After removal of the Ni, free-standing foams composed of conjoined hollow ultrathin graphite spheres are obtained. Control over the pore size and foam thickness is demonstrated. The graphitic foam is tested as a supercapacitor electrode, exhibiting electrochemical double-layer capacitance values that compare well to those obtained with the state-of-the-art 3D graphene materials.

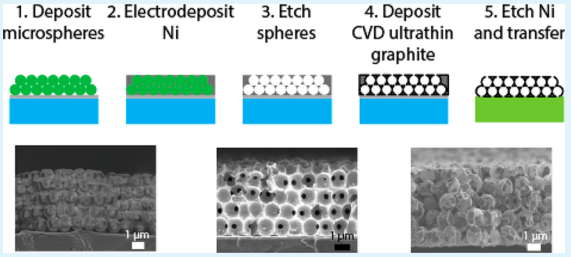

KEYWORDS: *graphene, ultrathin graphite, supercapacitors, templated electrodeposition, Langmuir–Blodgett, microsphere array*

Three-dimensional graphene and ultrathin graphite architectures have been proposed for a variety of applications, including chemical sensing, catalysis, hydrogen storage, and electrochemical energy storage.[1] The assembly of 2D graphene sheets into 3D structures is attractive for these applications due to the high conductivity and specific surface area of graphene and good mass transport provided by a 3D network. For supercapacitor applications, in particular, this 3D graphene architecture is desirable as an electrode material, due to its high porosity (hence, good ion transport) and high electrical conductivity (hence, good electrical transport), as well as its high surface area to mass ratio. Additionally, the carbon material is amenable to surface modifications and active material deposition, which can increase the total energy density through pseudocapacitive reactions.[2−4]

Previous efforts to fabricate 3D graphene structures are reviewed in ref 1. and include the chemical vapor deposition (CVD) growth of graphene on commercial Ni foams[5−7] and the self-assembly of graphene oxide flakes onto sacrificial polymer microsphere templates.[8−10] The former technique provides the advantage of relatively pristine graphene growth using CVD but yields a mediocre specific surface area due to the large (∼100 μm) pore size, while the latter allows for controlled pore size distribution and hierarchical architectures through microsphere size selection but yields an incompletely reduced graphene. In both cases, the template material can be removed to yield a lightweight, conductive, porous carbon material that is flexible[5] and can be used as supercapacitor[6,10] or battery[7] electrodes with good electrochemical performance. Moreover, these materials can be used in the absence of binders, conductive fillers, or additional current collectors, which increases the proportion of electrochemically active material in a device.

In this paper, we describe a new method to fabricate a bicontinuous 3D ultrathin graphite foam of controlled geometry through CVD-based growth on a templated electrodeposited Ni scaffold. "Ultrathin graphite" is used instead of "graphene" because of the multilayer nature of the fabricated films. The method involves electrodeposition of Ni into the pores of an ordered array of polymeric microspheres, followed by the etching of the spheres, deposition of graphitic layers, and the removal of Ni. As a practical demonstration of the utility of the technique, the resulting material is then tested as a supercapacitor electrode material.

The fabrication of the free-standing 3D ultrathin graphite foam is schematically illustrated in Figure 1 and briefly

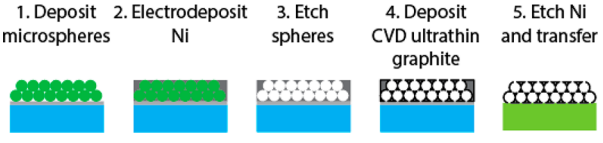

Figure 1. Schematic illustration of templated ultrathin graphite foam fabrication.

summarized below. Detailed methods are given in the Supporting Information. First, a 3D opaline array of polystyrene (PS) microspheres is deposited onto a conductive substrate. Many methods exist for the controlled deposition of microspheres into closely packed arrays on planar substrates.[11,12] In this paper, for depositions of the sphere layers, a Langmuir–Blodgett sequential dip coating process is used for good control of the number of layers.[13,14] Next, Ni is

Received: July 17, 2014
Accepted: October 15, 2014
Published: October 15, 2014

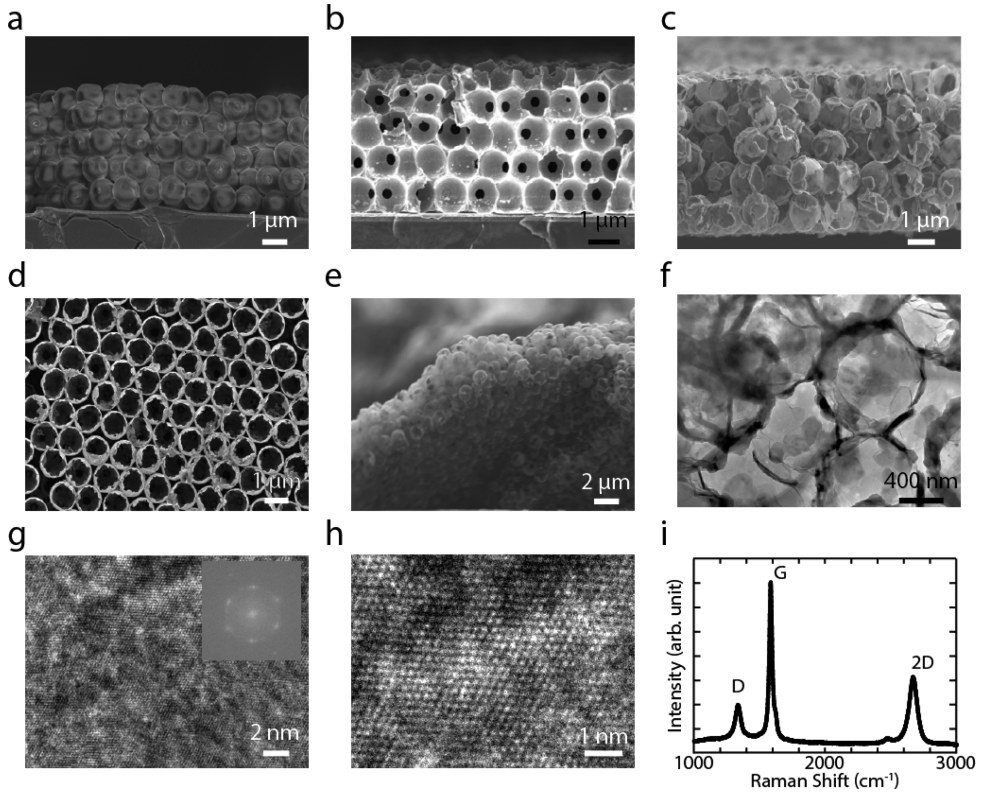

Figure 2. SEM images of (a) deposited polystyrene spheres with diameter of 1 μm (side view); (b) nickel scaffold after polystyrene removal (side view); (c) corresponding 3D ultrathin graphite foam (side view); (d) 3D ultrathin graphite foam (top view); (e) freestanding 3D ultrathin graphite foam. (f) TEM image of 3D ultrathin graphite foam. (g) Higher-magnification TEM image with Fourier transform inset. (h) TEM showing honeycomb graphitic lattice. (i) Raman spectrum of ultrathin graphite foam (excitation wavelength, 633 nm).

electrodeposited onto the sample and the PS is removed to form a reverse-opal scaffold (inspired by ref 15). A high throwing power Ni sulfate bath is used for the electrodeposition[16] and the PS spheres are dissolved using tetrahydrofuran. After that, ultrathin graphite is deposited onto the Ni scaffold via CVD. The high temperatures (1000−1050 °C) used in typical CVD graphene growth with a CH_4 precursor[5−7] are unsuitable for this technique, as the reverse opal electrodeposited structure is found to collapse at temperatures >600 °C. Therefore, benzene is used as the precursor to deposit the graphitic layer at 600 °C.[17] Finally, the Ni is etched in concentrated HCl to yield a free-standing foam composed of conjoined hollow ultrathin graphite spheres, which can be transferred to arbitrary substrates.

Scanning electron microscopy (SEM, Zeiss Gemini Ultra-55) and transmission electron microscopy (TEM, Philips CM300FEG/UT) are used to examine the morphological characteristics of the material during and after the fabrication process. Figure 2a shows a representative cross-sectional SEM image of a 5-layer ordered array of polystyrene spheres, 1 μm diameter, deposited on Ni-coated Si. Uniform, high packing density was obtained over a large sample area. Figure 2b shows the sample after Ni electrodeposition and polystyrene removal, showing a good fidelity "negative" reproduction of the original sphere template. The circular holes in the Ni scaffold correspond to the areas where adjacent polystyrene spheres sintered together. The carbon foam after Ni removal and transfer to polycarbonate sheet is shown in Figure 2c−e. The resulting foam shows a good reproduction of the original sphere morphology, with pores that correspond to the holes in the Ni scaffold. These pores allow for good ion transport and utilization of both "sides" of the graphene spheres. The hollow graphitic spheres also show variation in thickness along the shell of the sphere, indicating a polycrystalline growth of ultrathin graphite, as expected for CVD growth on Ni with a relatively slow cooling rate.[7]

Figure 2f shows a TEM image of an area of graphitic foam which has been mechanically agitated and drop cast onto a TEM grid such that only one layer of hollow spheres is visible. The observed spheres appear to have numerous crystalline grain boundaries and variable shell thickness, with a maximum shell thickness of ∼50 nm (which corresponds to ∼150 graphene layers). The significant variation in the thickness of the graphitic layer is apparent in both the SEM and TEM images. This is to be contrasted to the graphitic layers grown on Ni foams by Ji et al., which have a thickness on the order of 17 nm.[7] The difference in thickness likely arises from the difference in growth parameters, particularly the use of benzene vs methane as the precursor. Higher-magnification TEM images of a relatively thin region of a sphere are shown in Figures 2g, h. These images and the corresponding Fourier transforms show a regular honeycomb lattice with a lattice parameter of about 0.22 nm. This value is within 10% of the known lattice constant of graphite, 0.246 nm. This small deviation may be explained by the curved film being imaged with the electron beam likely not completely normal to the imaged layer.

Raman spectroscopy (HORIBA Jobin Yvon LabRam) is used to further confirm the graphitic nature of the carbon network. Figure 2i shows a representative Raman spectrum that displays the signature G and 2D peaks of graphitic carbons. The large G to 2D intensity ratio indicates multilayer graphene,[18] and the presence of a D peak indicates defects in the graphitic carbon.

Although Li et al. showed minimal D peak intensity for graphene grown on Cu foils using benzene at a growth temperature as low as 300 °C,[17] in this work, the D peak is present even at growth temperatures of 600 °C. This difference is likely due to the relatively low quality of electrodeposited Ni compared to Cu foils.

For electrochemical testing as supercapacitor electrodes, electrical connection to the foam is made via Cu wires attached with silver epoxy. The silver epoxy is coated with a nonconducting resin to prevent contact with the electrolyte. Three-electrode testing (Pt counter and Ag/AgCl reference electrodes) is performed using a CH Instruments potentiostat in an aqueous 3.5 M KCl electrolyte. Cyclic voltammetry at a variety of scan rates is performed on all fabricated foams. Some representative CV cycles are shown in Figure 3a. A semi-

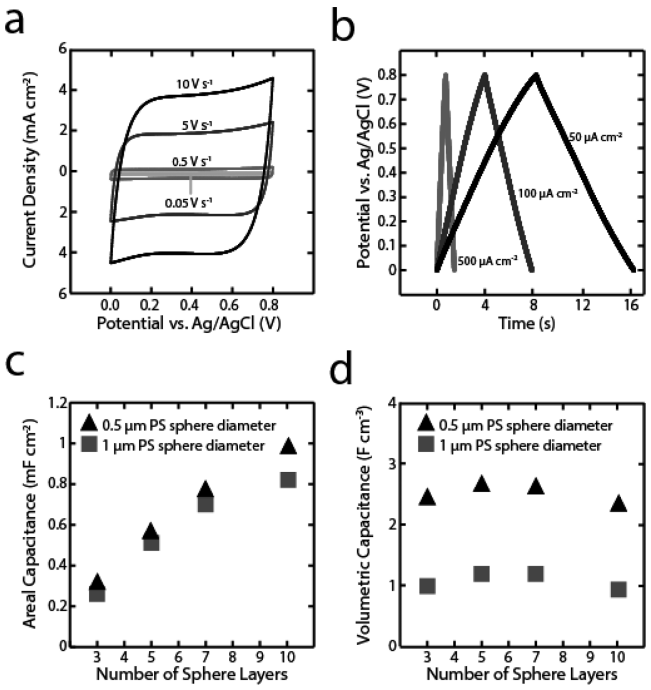

Figure 3. (a) Cyclic voltammogram of 5-layer, 1 um diameter sphere sample at different scan rates; (b) galvanostatic charge−discharge plots at various current densities; (c) the calculated areal and (d) volumetric capacitances for all fabricated samples, calculated from CV data at a scan rate of 50 mV/s.

rectangular plot can be seen at 0−0.8 V vs Ag/AgCl in both the cathodic and anodic regions. Galvanostatic charge−discharge plots (Figure 3b) show similar results; a pseudolinear discharge curve is apparent with slight nonlinearity apparent at similar potentials as the features seen in CV. The specific capacitance of the foams can be calculated via

$$C = \frac{I}{\Delta V/\Delta t A_{\text{proj}}} \tag{1}$$

where C is the specific areal capacitance, I is the average discharge current, $\Delta V/\Delta t$ is the average potential sweep rate during discharge, and A_{proj} is the projected area of the sample. The volumetric capacitance can be simply calculated by dividing by the thickness of the foam. Panels c and d in Figure 3 show the calculated areal and volumetric capacitances for all fabricated samples, calculated from the CV data at a scan rate of 50 mV/s. From simple geometric considerations, the specific surface area per projected area, A_A, of a close packed array of hollow spheres can be calculated using

$$A_A = \frac{2n(4\pi r^2)N}{A_{\text{proj}}} \tag{2}$$

where n is the number of layers of spheres, r is the sphere radius, and N is the number of spheres per layer in the projected area. The first factor of 2 is present to account for both the inside and outside surfaces of the hollow sphere. Equation 3 gives the relationship between N and A_{proj} assuming dense packing

$$N = \frac{A_{\text{proj}}}{\pi r^2}\frac{\pi}{2\sqrt{3}} \tag{3}$$

where the second term is the hexagonal packing density of circles in a plane. Combining eqs 2 and 3 yields

$$A_A = \frac{4\pi n}{\sqrt{3}} \tag{4}$$

revealing that the specific surface area per projected area, and hence the specific areal capacitance is expected to increase linearly with the number of layers. Figure 3c reflects this result, indicating that no significant transport losses are seen even for the thickest measured electrodes. Similarly, the volumetric specific area can be calculated via

$$A_V = \frac{2n(4\pi r^2)N}{A_{\text{proj}}t} = \frac{4\pi n}{\sqrt{3}\,t} \tag{5}$$

where t is the electrode thickness. For a close packed sphere array, t is given by

$$t = \left(\frac{2\sqrt{6}}{3}r\right)(n-1) + 2r \approx \left(\frac{2\sqrt{6}}{3}r\right)n \text{ for large } n \tag{6}$$

Combining eqs 5 and 6 yields

$$A_V \approx \frac{\pi\sqrt{2}}{r} \tag{7}$$

showing that A_V and hence the specific volumetric capacitance is mostly independent of the number of layers and depends only on the sphere size. Figure 3d qualitatively reflects this behavior. The calculated theoretical specific surface area per volume is 8.9 m^2/cm^3 for 0.5 μm diameter spheres; this is about 1 order of magnitude higher than the corresponding value for ∼9 layer CVD graphene grown on Ni foams[6] because of the smaller pore volume for the microsphere templated Ni scaffolds as compared to commercial Ni foams. Theoretically, this area could be further increased with decreasing sphere size. While specific surface area measurement techniques (such as BET) were attempted on the fabricated foams, the quantity of material was insufficient to generate a meaningful result. However, using the measured capacitances and the theoretical specific surface areas per volume, an approximate capacitance per real surface area of ∼20−30 $\mu F/cm^2$ is derived. This capacitance is 2−8 times higher than the typical double layer capacitance of carbon-based electrodes,[19] indicating that the actual specific surface area may be somewhat higher than the value calculated in eq 7. The difference in capacitance values likely arises from the roughness of the spherical surface giving a higher surface area than that of smooth spherical surfaces

assumed in the model used here. Thus, eq 7 likely gives a lower bound on the actual specific surface area per volume.

The highest measured areal capacitance of 1 mF/cm^2 is achieved on the 10-layer sample of 0.5 μm diameter spheres. The highest measured volumetric capacitance of 2.7 F/cm^3 is achieved on the 5 layer sample of 0.5 μm diameter spheres. The samples presented here show capacitance on the same order of magnitude as state-of-the-art 3D graphitic materials such as photoresist-derived carbon[20] and laser-scribed graphene.[21] Although these values should not be compared directly, as ref 21. reports results from a completed device in a two-electrode measurement, the order of magnitude similarity nevertheless shows the applicability of this technique for energy storage applications. The maximum calculated volumetric energy and power densities for the 5 layer, 1 μm diameter sample in a three-electrode configuration are 382 mJ/cm^3 and 3.2 W/cm^3 (see the Supporting Information for calculation), which are comparable to other novel 3D graphitic materials. The areal and volumetric energy and power densities are, in theory, further scalable with increasing thickness and decreasing sphere radius, respectively. While capacitance values normalized by projected area and volume are more appropriate for micro-supercapacitor applications,[22] this material may prove useful for both microscale and macro-scale applications, where a mass-normalized capacitance is more frequently cited. Although we expect the capacitance per mass to be quite high for this material (similar or higher to that of graphitic foams derived from commercial Ni foams), we were unable to synthesize a sufficient quantity of material to obtain a precise mass.

In conclusion, ultrathin graphite growth on a templated electrodeposited Ni layer is used to fabricate close-packed hollow 3D graphitic bicontinuous foam. This methodology can be extended to realize complex 3D graphitic architectures. These structures can be used for a variety of applications, and one such application, capacitive energy storage, is demonstrated here. The fabricated material shows promising electrochemical performance as well as scalability for supercapacitor applications. Furthermore, this technique can be extended to arbitrary templates to give excellent geometric control of 3D nanostructures at various length scales. The only requirement is that the template be amenable to electrodeposition of Ni. Instead of being used to create the structures shown here, the process may be used to generate myriad graphitic carbon structures including block copolymer templated gyroids, hierarchically porous films, and controlled diameter nanotubes. These structures could be engineered for specific applications through modification of the graphitic structures, taking advantage of the unique properties of graphene, as well as the control afforded by a templated fabrication.

■ ASSOCIATED CONTENT

Ⓢ Supporting Information

Experimental details. This material is available free of charge via the Internet at http://pubs.acs.org.

■ AUTHOR INFORMATION

Corresponding Author

*E-mail: maboudia@berkeley.edu.

Author Contributions

†B.H., M.S.K., and L.E.L. contributed equally to this work.

Notes

The authors declare no competing financial interest.

■ ACKNOWLEDGMENTS

The authors thank Seung Hoon Lee, Shuang Wang and John Alper for many fruitful discussions. The financial support of National Science Foundation (Grants EEC-0832819, Center of Integrated Nanomechanical Systems, and DMR-1207053) is gratefully acknowledged. SEM and TEM work at the Molecular Foundry was supported by the Office of Science, Office of Basic Energy Sciences, of the U.S. Department of Energy under Contract No. DE-AC02-05CH11231. B.H. and L.E.L. also acknowledge NSF Graduate Research Fellowships.

■ REFERENCES

(1) Li, C.; Shi, G. Three-Dimensional Graphene Architectures. *Nanoscale* **2012**, *4*, 5549−5563.

(2) Frackowiak, E. Carbon Materials for Supercapacitor Application. *Phys. Chem. Chem. Phys.* **2007**, *9*, 1774−1785.

(3) Chen, S.; Zhu, J.; Wu, X.; Han, Q.; Wang, X. Graphene Oxide-MnO2 Nanocomposites for Supercapacitors. *ACS Nano* **2010**, *4*, 2822−2830.

(4) Jiang, J.; Li, Y.; Liu, J.; Huang, X.; Yuan, C.; Lou, X. W. Recent Advances in Metal Oxide-based Electrode Architecture Design for Electrochemical Energy Storage. *Adv. Mater.* **2012**, *24*, 5166−5180.

(5) Chen, Z.; Ren, W.; Gao, L.; Pei, S.; Cheng, H.-M. Three-Dimensional Flexible and Conductive Interconnected Graphene Networks Grown by Chemical Vapour Deposition. *Nat. Mater.* **2011**, *10*, 424−428.

(6) Cao, X.; Shi, Y.; Shi, W.; Lu, G.; Huang, X.; Yan, Q.; Zhang, Q.; Zhang, H. Preparation of Novel 3D Graphene Networks for Supercapacitor Applications. *Small* **2011**, *7*, 3163−3168.

(7) Ji, H.; Zhang, L.; Pettes, M. T.; Li, H.; Chen, S.; Shi, L.; Piner, R.; Ruoff, R. S. Ultrathin Graphite Foam: a Three-Dimensional Conductive Network for Battery Electrodes. *Nano Lett.* **2012**, *12*, 2446−2451.

(8) Vickery, J. L.; Patil, A. J.; Mann, S. Fabrication of Graphene-Polymer Nanocomposites with Higher-Order Three-Dimensional Architectures. *Adv. Mater.* **2009**, *21*, 2180−2184.

(9) Hong, J.; Char, K.; Kim, B.-S. Hollow Capsules of Reduced Graphene Oxide Nanosheets Assembled on a Sacrificial Colloidal Particle. *J. Phys. Chem. Lett.* **2010**, *1*, 3442−3445.

(10) Choi, B. G.; Yang, M.; Hong, W. H.; Choi, J. W.; Huh, Y. S. 3D Macroporous Graphene Frameworks for Supercapacitors with High Energy and Power Densities. *ACS Nano* **2012**, *6*, 4020−4028.

(11) Stein, A. Sphere Templating Methods for Periodic Porous Solids. *Microporous Mesoporous Mater.* **2001**, *44*−*45*, 227−239.

(12) Xia, Y.; Gates, B.; Yin, Y.; Lu, Y. Monodispersed Colloidal Spheres: Old Materials with New Applications. *Adv. Mater.* **2000**, *12*, 693−713.

(13) Liu, Z.; Ya, J.; Xin, Y.; Ma, J.; Zhou, C. Assembly of Polystyrene Colloidal Crystal Templates by a Dip-Drawing Method. *J. Cryst. Growth* **2006**, *297*, 223−227.

(14) Lee, D. H.; Kim, Y.; Fearing, R. S.; Maboudian, R. Effect of Fiber Geometry on Macroscale Friction of Ordered Low-Density Polyethylene Nanofiber Arrays. *Langmuir* **2011**, *27*, 11008−11016.

(15) Zhang, H.; Yu, X.; Braun, P. V. Three-Dimensional Bicountinuous Ultrafast-Charge and -Discharge Bulk Battery Electrodes. *Nat. Nanotechnol.* **2011**, *6*, 277−281.

(16) Di Bari, G. A., In *Modern Electroplating*; Schlesinger, M., Paunovic, M., Eds.; John Wiley & Sons, Inc.: Hoboken, NJ, 2010; Chapter 3, pp 79−114.

(17) Li, Z.; Wu, P.; Wang, C.; Fan, X.; Zhang, W.; Zhai, X.; Zeng, C.; Li, Z.; Yang, J.; Hou, J. Low-Temperature Growth of Graphene by Chemical Vapor Deposition Using Solid and Liquid Carbon Sources. *ACS Nano* **2011**, *5*, 3385−3390.

(18) Ferrari, A. C.; Meyer, J. C.; Scardaci, V.; Casiraghi, C.; Lazzeri, M.; Mauri, F.; Piscanec, S.; Jiang, D.; Novoselov, K. S.; Roth, S.; Geim, A. K. Raman Spectrum of Graphene and Graphene Layers. *Phys. Rev. Lett.* **2006**, *97*, 187401.

(19) Ji, H.; Zhao, X.; Qiao, Z.; Jung, J.; Zhu, Y.; Lu, Y.; Zhang, L. L.; MacDonald, A. H.; Ruoff, R. S. Capacitance of Carbon-Based Electrical Double-Layer Capacitors. *Nat. Commun.* **2014**, *5*, 3317.
(20) Hsia, B.; Kim, M. S.; Vincent, M.; Carraro, C.; Maboudian, R. Photoresist-Derived Porous Carbon for On-Chip Micro-Supercapacitors. *Carbon* **2013**, *57*, 395−400.
(21) El-Kady, M. F.; Kaner, R. B. Scalable Fabrication of High-Power Graphene Micro-Supercapacitors for Flexible and On-Chip Energy Storage. *Nat. Commun.* **2013**, *4*, 1475.
(22) Gogotsi, Y.; Simon, P. True Performance Metrics in Electrochemical Energy Storage. *Science* **2011**, *334* (6058), 917−918.